Metabotropic glutamate receptor subtype 2 is a receptor of SARS-CoV-2

Zhigao Bu (buzhigao@caas.cn)
Harbin Veterinary Research Institute, CAAS https://orcid.org/0000-0001-9242-4211

Jinliang Wang
Harbin Veterinary Research Institute, CAAS https://orcid.org/0000-0002-5034-8131

Guan Yang
Beijing Institute of Lifeomics

Xinxin Wang
Harbin Veterinary Research Institute, CAAS

Zhiyuan Wen
Harbin Veterinary Research Institute, CAAS https://orcid.org/0000-0003-3112-0243

Lei Shuai
Harbin Veterinary Research Institute, CAAS https://orcid.org/0000-0003-2122-8365

Jie Luo
Harbin Veterinary Research Institute, CAAS

Chong Wang
Harbin Veterinary Research Institute, CAAS https://orcid.org/0000-0002-3970-9071

Ziruo Sun
Harbin Veterinary Research Institute, CAAS

Renqiang Liu
Harbin Veterinary Research Institute, CAAS https://orcid.org/0000-0001-6456-812X

Jinying Ge
Harbin Veterinary Research Institute, CAAS

Xijun He
Harbin Veterinary Research Institute, CAAS

Qianqian He
Harbin Veterinary Research Institute, CAAS

Xijun Wang
Harbin Veterinary Research Institute, CAAS

Xiao Yang
State Key Laboratory of Proteomics, Beijing Proteome Research Center, National Center for Protein Sciences, Beijing Institute of Lifeomics https://orcid.org/0000-0002-0298-9831

Weiye Chen
Harbin Veterinary Research Institute, CAAS

Gongxun Zhong
State key Laboratory of Veterinary Biotechnology, Harbin Veterinary Research Institute
https://orcid.org/0000-0002-0748-9641

Biological Sciences - Article

Keywords: SARS-CoV-2, ACE2, metabotropic glutamate receptor subtype 2

Posted Date: April 21st, 2021

DOI: https://doi.org/10.21203/rs.3.rs-301270/v1

Metabotropic glutamate receptor subtype 2 is a receptor of SARS-CoV-2

Jinliang Wang[1, ‡], Guan Yang[2, ‡], Xinxin Wang[1, ‡], Zhiyuan Wen[1], Lei Shuai[1], Jie Luo[1], Chong Wang[1], Ziruo Sun[1], Renqiang Liu[1], Jinying Ge[1], Xijun He[1], Qianqian He[1], Xijun Wang[1], Xiao Yang[2], Weiye Chen[1], Gongxun Zhong[1] and Zhigao Bu[1, *]

[1]State Key Laboratory of Veterinary Biotechnology, Harbin Veterinary Research Institute, Chinese Academy of Agricultural Sciences, Harbin 150069, P. R. China.

[2]State Key Laboratory of Proteomics, Beijing Proteome Research Center, National Center for Protein Sciences (Beijing), Beijing Institute of Lifeomics, Beijing 102206, P. R. China.

[*]Correspondence: buzhigao@caas.cn (Z.B.)

[‡]These authors contributed equally to this work.

Abstract

Severe acute respiratory syndrome coronavirus 2 (SARS-CoV-2) is the causative pathogen of novel coronavirus disease 2019 (COVID-19)[1]. SARS-CoV-2 uses angiotensin converting enzyme 2 (ACE2) as a cellular receptor and enters cells via clathrin-mediated endocytosis (CME)[2-4]. However, the key molecules involved in internalizing and facilitating CME for virus entry remain unknown. Here, we found metabotropic glutamate receptor subtype 2 (mGluR2) is a key entry receptor for SARS-CoV-2 infection. mGluR2 directly interacts with the SARS-CoV-2 spike protein. Knockdown of mGluR2 decreases endocytosis of SARS-CoV-2 but not cell binding. mGluR2 cooperates with ACE2 to facilitate SARS-CoV-2 entry through CME. Knockout of the mGluR2 gene in mice abolished SARS-CoV-2 infection in the nasal turbinates and significantly reduced viral infection in the lungs. Importantly, mGluR2 also is important for severe acute respiratory syndrome coronavirus spike protein and Middle East respiratory syndrome coronavirus spike protein mediated endocytosis. Our study provides important insights into SARS-CoV-2 infection and reveals an important target for the development of novel approaches to limit coronavirus infection.

Main

A novel coronavirus named severe acute respiratory syndrome coronavirus 2 (SARS-CoV-2) was identified as the causative pathogen of novel coronavirus disease 2019 (COVID-19)[1]. SARS-CoV-2 is an enveloped, non-segmented positive-stand RNA virus, belonging to the coronaviridae family, which consists of four genera: *alphacoronavirus, betacoronavirus, gammacoronavirus,* and *deltacoronavirus*[5]. Human coronaviruses usually cause mild respiratory tract infections; however, severe acute respiratory syndrome coronavirus (SARS-CoV), Middle East respiratory syndrome coronavirus (MERS-CoV), and SARS-CoV-2, which all belong to the genus *betacoronavirus*[6], can cause severe disease and death in humans.

The first step in coronavirus infection is binding to cellular receptors via the viral envelope Spike (S) protein[6]. The S protein is composed of the S1 and S2 subdomains. The S1 subdomain contains the receptor-binding domain (RBD) and is responsible for binding to specific receptors. The S2 subdomain contains a fusion peptide and is responsible for the fusion of the viral membrane with the cellular membrane[6,7]. In addition to angiotensin converting enzyme 2 (ACE2), other proteins have been reported to be involved in SARS-CoV-2 infection by affecting viral attachment and entry; these proteins include heparan sulfate, neuropilin 1, tyrosine-protein kinase receptor UFO, and HDL-scavenger receptor B type 1[8-12].

mGluR2 is a receptor of SARS-CoV-2

Metabotropic glutamate receptor 2 (mGluR2) is an important seven-transmembrane domain receptor and is thought to be functionally involved in cognitive disorders, drug addiction, psychosis, schizophrenia, anxiety, cerebral ischemia, and epilepsy[13-16]. Previous study found that mGluR2 facilitates rabies virus to enter cells[17], suggesting that mGluR2 plays a role in virus infection. To test whether mGluR2 is needed for SARS-CoV-2 infection, we first tested mGluR2 expression by flow cytometry in Vero-E6 cells and Caco-2 cells, which are susceptible to SARS-CoV-2 infection. mGluR2 was labeled on the cell membrane of the two cell lines and examined by using flow cytometry. Results showed that both cell lines expressed mGluR2 on the cell surface (Extended Data Fig. 1a, b). We then knocked down mGluR2 expression by transfecting Vero-E6 cells and Caco-2 cells with the specific siRNA to mGluR2 mRNA. Compared with cells mock-transfected with non-targeting siRNA, the expression of mGluR2 mRNA was significantly reduced in both cell types at 18 h after transfection (Fig. 1a). At 72 h post-transfection, Vero-E6 cells (MOI=0.01) and Caco-2 cells (MOI=0.05) were each infected with a SARS-CoV-2 human isolate (HRB25). The culture supernatants of the infected cells were detected by viral titration at 24 h post-infection (p.i.). Knockdown of mGluR2 significantly decreased the viral titers in both cells (Fig. 1b). The mGluR2 expression was also found on the surface of the primary human pulmonary alveolar epithelial cells (HPAE cells) (Extended Data Fig. 1c), and knockdown of mGluR2 significantly decreases the viral RNA level in the cell lysate (MOI=0.001) (Fig. 1a, c). These results suggest that mGluR2 is required for SARS-CoV-2 infection.

To investigate whether mGluR2 is a potential receptor for SARS-CoV-2 infection, we used co-immunoprecipitation assays to ask whether mGluR2 interacts with the SARS-CoV-2 S protein. Flag-tagged mGluR2 (mGluR2-Flag) was co-expressed with Myc-tagged S protein (S-Myc) in plasmid-transfected HEK293 cells. Immunoblotting for S-Myc demonstrated that mGluR2 interacts with the SARS-CoV-2 S protein specifically (Fig. 1d). To characterize the domain of the SARS-CoV-2 S protein that interacts with mGluR2, we performed a co-immunoprecipitation analysis using the S1 subdomain and the RBD of the SARS-CoV-2 S protein in plasmid-transfected HEK293 cells. We found that both the S1 and RBD interacted with mGluR2 (Fig. 1e, f). We then performed pull-down assays to determine whether mGluR2 interacts with the SARS-CoV-2 S protein directly. Purified recombinant GST-tagged ectodomain of mGluR2 (mGluR2-GST) was pooled with lysate from HEK293 cells transfected with the SARS-CoV-2 S protein, S1 subdomain, or RBD, respectively. We found that purified mGluR2-GST successfully pulled down the SARS-CoV-2 S protein, S1 subdomain and RBD (Fig. 1g-1i). These results demonstrate that the ectodomain of mGluR2 interacts directly with the RBD of the SARS-CoV-2 S protein.

To investigate whether mGluR2 serves as a receptor for SARS-CoV-2 infection, we tested whether an antibody to the ectodomain of mGluR2 could block SARA-CoV-2 infection in vitro. Vero-E6 cells and Caco-2 cells were treated with the mGluR2 antibody at different concentrations for 1 h at 4°C, and then incubated with HRB25. Infectious titers in the supernatant were detected by virus titration at 48 h p.i.. The result showed that the mGluR2 antibody efficiently inhibited SARS-CoV-2 infection in a dose-dependent manner in Vero-E6 and Caco-2 cells (Fig. 1k). The cytotoxicity of the mGluR2 antibody in both cell types was also tested, and the results confirmed that the cell viability was unaffected even at the highest concentration used (Fig. 1j). We confirmed the results in HPAE cells and found that mGluR2 antibody has no cytotoxicity at the concentration used (Fig. 1j) and significantly decreases the viral RNA level in the cell lysate (Fig. 1l).

We then tested whether mGluR2 could block SARS-CoV-2 infection *in vitro*. SARS-CoV-2 was pooled with different concentrations of mGluR2-GST for 1 h at 4°C, then Vero-E6 cells were incubated with the mixtures for 1 h at 37°C. The infectious titers in the supernatants of the infected cells were detected by virus titration at 24 h p.i.. mGluR2-GST showed an inhibitory effect in a dose-dependent manner (Fig. 1m). Together, these results suggest that mGluR2 is a functional receptor for SARS-CoV-2 infection.

SARS-CoV-2 endocytosis requires mGluR2

We next tested which stage of SARS-CoV-2 entry was mediated by mGluR2. We performed mGluR2 RNAi assays to determine whether knocking down mGluR2 expression affected the binding or internalization of SARS-CoV-2. mGluR2-silenced Vero-E6 cells and Caco-2 cells and control cells were incubated with HRB25 at 4ºC for 1 h and washed to remove unbound virus. Then the cells were shifted to 37ºC for 1 h to allow the endocytosis of bound viruses. The cells were washed with normal PBS or acid buffer/trypsin, which could efficiently remove cell surface-bound SARS-CoV-2 on both cell lines (Extended Data Fig. 2a, b). The washed cells were lysed for qPCR detection of SARS-CoV-2 bound to the cell surface or

entered the cells. The viruses bound on the mGluR2-silenced cells were comparable with those of the control cells, however, the viruses entered the mGluR2-silenced cells were significantly less than those in the control cells (Fig. 2a, b), indicating that mGluR2 silence affected the endocytosis of SARS-CoV-2 while having no effect on binding in both cell types.

To verify these results, we performed a microscopy-based assay to monitor the endocytosis of SARS-CoV-2. Vero-E6 cells were processed as described above except for the acid buffer/trypsin wash. The cells were incubated with an antibody against the SARS-CoV-2 S protein under unpermeabilized or permeabilized conditions, and stained to visualize viral particles. The fluorescence intensity of each cell was calculated. The fluorescence intensity under unpermeabilized conditions indicates how many viral particles were unable to enter the cells, whereas that under permeabilized conditions indicates the total number of viral particles. We found that the fluorescence intensity in mGluR2-silenced Vero-E6 cells was significantly higher than that in scrambled siRNA-transfected cells under unpermeabilized conditions, but similar to that of scrambled siRNA-transfected cells under permeabilized conditions (Fig. 2c). These results confirm that mGluR2 is required for the endocytosis of SARS-CoV-2 but not cell binding.

We next investigated whether mGluR2 is internalized with SARS-CoV-2. The expression of mGluR2 on the cell surface before and after infection with SARS-CoV-2 was first quantitatively determined by flow cytometry under unpermeabilized conditions. The results showed that SARS-CoV-2 infection leads to a significant decrease in the cell surface expression of mGluR2 (Fig. 2d), indicating that mGluR2 was internalized upon infection. It has been suggested that SARS-CoV-2 can enter host cells through CME[2]. We therefore observed the subcellular localization of SARS-CoV-2 particles, mGluR2 and clathrin by using multiplex immunofluorescence staining in HRB25-infected Vero-E6 cells and HPAE cells as previously described[17]. We found that SARS-CoV-2 particles, mGluR2, and clathrin co-localize in infected cells (Fig. 2e, f), which indicates that the SARS-CoV-2-mGluR2 complex internalizes together.

mGluR2 interacts with ACE2

ACE2 is now well characterized as a receptor for SARS-CoV-2 binding to cells[4]. We demonstrated that SARS-CoV-2 infection does not affect the cell surface expression of ACE2 (Fig. 2g), which indicates that ACE2 does not internalize with SARS-CoV-2. Therefore, ACE2 might pass the virus to mGluR2 to mediate endocytosis. A direct interaction between mGluR2 and ACE2 would strongly support the hypothesis. The result from co-immunoprecipitation assays found that mGluR2 interacts with ACE2 (Fig. 2h). Pull-down assays demonstrated that the ectodomain of mGluR2 interacts with ACE2 directly (Fig. 2i). We further performed multiplex immunofluorescence to detect SARS-CoV-2, ACE2 and mGluR2 in HRB25-infected Vero-E6 cells. Result showed that ACE2, SARS-CoV-2 and mGluR2 co-localize in cells (Fig. 2j).

mGluR2 expresses in respiratory system

mGluR2 is known to be expressed mainly in neurons[18]. To investigate the distribution of

mGluR2 in cells of respiratory tract, we performed multiplex immunofluorescence staining on normal human lung sections, mouse turbinate sections, and mouse lung sections. In human lung, the mGluR2 expression was found in SPC^+ alveolar type II cells and $Tubb4^+$ ciliated cells, and ACE2 expression was also detected in these cells (Fig. 3a, b). In nasal turbinates of mice, relatively high mGluR2 expression was detected in $CK8^+$ sustentacular cells and OMP^+GAP43^+ olfactory neurons, whereas Ace2 expression were limited to $CK8^+$ cells in olfactory epithelium (Fig. 3c). In the lungs of mice, mGluR2 was mainly expressed in $CC10^+$ club cells, SPC^+ alveolar type II cells, and $Tubb4^+Foxj1^+$ ciliated cells (Fig. 3d).

We further performed multiplex immunofluorescence staining on turbinate section and lung section of mice that were infected with SARS-CoV-2 virus, and we found that SARS-CoV-2-infected cells were mainly $mGluR2^+$ cells. In nasal turbinates of mice, high level of SARS-CoV-2 N protein and mGluR2 expression were detected in $CK8^+$ sustentacular cells in olfactory epithelium (Fig. 3e). In the lungs, obvious colocalization of SARS-CoV-2 and mGluR2 was observed in some of SARS-CoV-2-infected $Ace2^+$ cells (Fig. 3f). These results indicate that mGluR2 is widely expressed in the cells of respiratory tract that could be infected by the SARS-CoV-2.

mGluR2 is a functional receptor in mice

We next asked whether mGluR2 is important for SARS-CoV-2 infection *in vivo*. mGluR2 gene knockout ($mGluR2^{-/-}$) mice were generated by using the CRISPR/Cas9 system (Extended Data Fig. 3a) and genotype was identified with PCR (Extended Data Fig. 3b). Twelve wild-type mice and 13 $mGluR2^{-/-}$ mice were intranasally inoculated with 150 PFU of the mouse-adapted HRM26M virus[19]. The viral RNA and infectious viruses in the nasal turbinates and lungs were detected at 3 days p.i. by qPCR and viral titration. Compared with wild-type mice, $mGluR2^{-/-}$ mice showed significantly decreased viral RNA copies in their nasal turbinates and lungs (Fig. 3g, i). Infectious virus was not detected in the nasal turbinates of $mGluR2^{-/-}$ mice (Fig. 3h) and the level of infectious virus was 100-times lower in the lungs of $mGluR2^{-/-}$ mice than that of wild-type mice (Fig. 3j).

Betacoronavirus entry requires mGluR2

SARS-CoV and MERS-CoV are also highly pathogenic coronaviruses to humans[6]. We therefore asked whether mGluR2 is important for SARS-CoV and MERS-CoV to enter cells. We first investigated whether the S proteins of SARS-CoV and MERS-CoV interact with mGluR2. Co-immunoprecipitation assays demonstrated that SARS-CoV S interacts with mGluR2 whereas MERS-CoV S does not interact with mGluR2 (Fig. 4a, b). DPP4, a known receptor of MERS-CoV[20], interacts with mGluR2 directly (Fig. 4c, d). For evaluate infection, recombinant vesicular stomatitis viruses (VSV) expressing SARS-CoV S (rVSV-SARS-CoV-S) or MERS-CoV S (rVSV-MERS-CoV-S) were used to substitute for authentic SARS-CoV and MERS-CoV, respectively. These two chimeric VSVs were generated by following the previously described strategy.[21], in which the open reading frame (ORF) of the G gene is replaced with the ORF of the SARS-CoV or MERS-CoV S gene. Antibodies against mGluR2 efficiently blocked the infections of rVSV-SARS-CoV-S (MOI=0.05) and rVSV-MERS-CoV-S (MOI=0.05) in Vero-E6 cells (Fig. 4f), but failed to

block the infection of VSV in Vero-E6 cells (Fig. 4e). We next examined the internalization of rVSV-SARS-CoV-S (MOI=10) and rVSV-MERS-CoV-S (MOI=10) in Vero-E6 cells. mGluR2 knockdown significantly decreased the endocytosis of both viruses but had no effect on binding to the cells (Fig. 4g, h, Extended Data Fig. 2c, d). Together, these results indicate that mGluR2 is important for the endocytosis of SARS-CoV and MERS-CoV.

Discussion

We, for the first time to our knowledge, demonstrate that mGluR2 is a bona fide functional receptor for SARS-CoV-2 infection. mGluR2 gene knockout prevented SARS-CoV-2 replication in the nasal turbinate of mice, which suggests that mGluR2 is a functional receptor for SARS-CoV-2 infection of the nasal turbinate. However, mGluR2 gene knockout did not completely prevent SARS-CoV-2 infection in the lungs, indicating that other entry receptors must also contribute to SARS-CoV-2 infection. Our results indicate that SARS-CoV-2 may use multiple receptors to enter cells in the lungs. mGluR2 also is important for SARS-CoV S protein and MERS-CoV S protein mediated endocytosis, which suggests that mGluR2 likely plays a conserved role in the entry of coronaviruses, at least betacoronavirus. Our findings should help further the development of novel approaches to inhibit coronavirus infection by targeting mGluR2.

Although human coronaviruses are typically associated with respiratory tract diseases, three human coronaviruses have been shown to infect neurons: HCoV-229E, HCoV-OC43, and SARS-CoV[22]. MERS-CoV has also been associated with neurological disease in some cases[23]. Increasing evidence indicates that SARS-CoV-2 not only affects the respiratory tract but also impacts the central nervous system, resulting in neurological symptoms, such as loss of smell and taste, headache, and nausea[24-26]. A recent study revealed that SARS-CoV-2 can enter the nervous system by crossing the neural-mucosal interface in the olfactory mucosa[27], which indicates that the nasal turbinate is an important access point for SARS-CoV-2 to enter the brain. In the present study, we found that mGluR2 is essential for SARS-CoV-2 infection of the nasal turbinate. Given that mGluR2 is widely expressed in neurons, we cannot exclude the possibility that mGluR2 is involved in SARS-CoV-2 neurotropism. Unfortunately, investigation of the role of mGluR2 in SARS-CoV-2 neurotropism is very difficult due to the lack of a suitable model in vitro and in vivo. The discovery of a role for mGluR2 in SARS-CoV-2 infection supports the possibility that SARS-CoV-2 could use mGluR2 to enter and infect neuron cells.

Methods

Cell lines

HEK293 cells (ATCC, CRL-1573), Caco-2 cells (ATCC; HTB-37), and Vero-E6 cells (ATCC, CRL-1586) were maintained in Dulbecco's modified Eagle's medium (DMEM) supplemented with 10% fetal bovine serum (FBS), 1% penicillin/streptomycin, and L-glutamine at 37°C in 5% CO_2. Human Pulmonary Alveolar Epithelial Cells (HPAE cells) (ScienCell Research Laboratories, 3200) were cultured in alveolar epithelial cell medium (ScienCell Research Laboratories, 3201).

Viruses

SARS-CoV-2/HRB25/human/2020/CHN (HRB25, GISAID access no. EPI_ISL_467430) and mouse-adapted SARS-CoV-2/HRB26/human/2020/CHN (HRB26M, GISAID access no. EPI_ISL_459910) were maintained in our laboratory. VSV chimeras expressing the S protein of SARS-CoV (rVSV-SARS-CoV-S) or MERS-CoV (rVSV-MERS-CoV-S) were generated as previously described [21]. Virus titers were determined by using standard plaque assays on Vero-E6 cells, and virus stocks were aliquoted and stored at −80°C until use. All experiments with infectious SARS-CoV-2 were performed in the biosafety level 4 and animal biosafety level 4 facilities in the Harbin Veterinary Research Institute (HVRI) of the Chinese Academy of Agricultural Sciences (CAAS).

Mice

All mice were bred on the C57BL/6J background. Six- to eight-week-old C57BL/6J mice were obtained from Vital River Laboratories (Vital River Laboratories, Beijing, China). mGluR2$^{-/-}$ mice were from the Model Animal Research Center of Nanjing University. mGluR2$^{-/-}$ mice were generated by crossing and using the CRISPR/Cas9 system. Cas9 mRNA and sgRNA were co-injected into zygotes. sgRNA (Table S1) directed Cas9 endonuclease cleavage upstream of exon 1 and the 3'UTR, creating a double-strand break. Such breaks were repaired by non-homologous end joining, which resulted in the destruction of the mGluR2 gene. Pups were genotyped by PCR, followed by sequence analysis. Mice were maintained under conventional conditions in the HVRI of CAAS, which is approved for such use by the Ministry of Agriculture and Rural Affairs of China. All institutional and national guidelines for the care and use of laboratory animals were followed. All mouse experiments were carried out in strict accordance with the recommendations in the Guide for the Care and Use of Laboratory Animals of the Ministry of Science and Technology of the People's Republic of China. The protocols were approved by the Committee on the Ethics of Animal Experiments of the HVRI of CAAS.

Plasmids

pCAGGS-mGluR2-Flag was described previously [17]. Human ACE2, and DPP4 cDNAs were prepared from the total RNA of HEK293 cells by RT-PCR, and then cloned into the pCAGGS-Flag and pCAGGS-Myc vectors as indicated in our study, and confirmed by sequencing analysis. The SARS-CoV-2 S gene (GenBank: MN908947.3), S1 subdomain (aa 14-685) and RBD (aa 331-524), SARS-CoV S gene (GenBank: AAP13441.1), and MERS-CoV S gene (GenBank: KF186567.1) were cloned into the pCAGGS-Myc vector and confirmed by sequencing analysis.

Flow cytometry

To detect mGluR2, Vero-E6 cells and Caco-2 cells were seeded onto 6-well plates. After 12 h, the cells were trypsinized with 0.25% trypsin (without EDTA) to harvest the cells. HPAE cells were seeded in 48-well plates for 72 h, then performed as above. To detect mGluR2 and ACE2 on the membrane after virus infection, Vero-E6 cells were seeded onto 6-well plates for 16 h and then infected with HRB25 (MOI= 5) at 4°C for 1 h or at 37˚C for 30 min. The cells

were then harvested as described above. The cells were fixed with 3% paraformaldehyde at room temperature for 15 min, then washed three times with FACS wash buffer (PBS containing 2% FCS), and incubated for 1 h with mGluR2 antibody (1:300, Santa Cruz Biotechnology, sc-271654), ACE2 antibody (1:1000, R&D system, AF933), IgG2a isotype antibody (1:1500, Southern Biotech, 0103-01), or IgG isotype antibody (1:1000, R&D system, AB-108-C), which served as a control. They were then washed and stained with goat anti-mouse Alexa Fluor 488 (1:1000, Thermo Fisher, A11034) or donkey anti-goat Alexa Fluor 488 (1:1000, Abcam, ab150129) for 1 h. All cells were analyzed by using a FC500 flow cytometer (Beckman Coulter). Cell surface mean fluorescence density was measured and analyzed by using FlowJo software (FlowJo LLC).

RNAi

siRNA transfections were performed by using the Lipofectamine RNAiMAX transfection reagent (Thermo Fisher Scientific, 13778150) according to the manufacturer's instructions. Briefly, siRNA (1 μM, 40 μl per well, African green monkey, Sigma or 1 μM, 30 μl per well, human, ambion) targeting the mGluR2, or non-targeting siRNA, was mixed with OptiMEM medium containing 0.8 μl of Lipofectamine RNAiMAX transfection reagent in a volume of 120 μl per well on 24-well plates. After a 30-min incubation at room temperature, Vero-E6 cells and Caco-2 cells were seeded into siRNA-coated 24-well plates in a volume of 500 μl per well. The RNAi assay of HPAE cells was performed with siRNA (1 μM, 20 μl per well, human, ambion) mixed with 80 μl OptiMEM medium containing 0.8 μl RNAiMAX in 48-well plates. At 18 h after the siRNA transfection, mGluR2 mRNA was assessed by qPCR. At 72 h post-transfection, the cells were infected with HRB25 for further studies. The siRNA sequences and the qPCR assay primers used to verify knockdown are listed in Table S1.

Plaque assay

Viral titers from the cell culture medium or animal tissues were determined by use of plaque-forming unit (PFU) assays. Serial dilutions of supernatants from infected cells or animal tissues homogenate were added to Vero-E6 cell monolayer and adsorbed for 1 h at 37°C. Cells were then washed and plaque media was overlaid on the cells, which were then placed at 37°C. After 48 h of incubation, the cell monolayers were stained with crystal violet and plaques were counted.

$TCID_{50}$ assay

Briefly, serial 10-fold dilutions of the virus supernatant were made and 100 μl of each dilution was added to Vero-E6 cells in quadruplicate of 96-well plates. The plates were incubated for 24 h at 37 °C and then the GFP-expressing cells were observed under a fluorescence microscope. The 50% tissue culture infective dose ($TCID_{50}$) was calculated by Reed & Muench.

Quantitative PCR (qPCR)

The viral RNA copies in the samples collected from animals were determined as described previously [28]. Briefly, viral RNA was extracted by using a QIAamp vRNA Minikit (Qiagen) and reverse transcription was performed by using the HiScript® II Q RT SuperMix for qPCR

(Vazyme). qPCR was conducted by using the Applied Biosystems® QuantStudio® 5 Real-Time PCR System (Thermo Fisher) with Premix Ex Taq™ (Probe qPCR), Bulk (TaRaKa), and SARS-CoV-2 N gene-specific primers (forward, 5'-GGGGAACTTCTCCTGCTAGAAT-3'; reverse, 5'-CAGACATTTTGCTCTCAAGCTG-3) and probe (5'-FAM-TTGCTGCTGCTTGACAGATT-TAMRA-3'). The amount of viral RNA for the target SARS-CoV-2 N gene was normalized to a standard curve obtained by using a plasmid (pBluescriptIISK-N, 4,221 bp) containing the full-length cDNA of the SARS-CoV-2 N gene.

To detect mGluR2 mRNA, and viral RNA in cells, total RNA from cells was isolated using TRIZOL reagent (Thermo Fisher) and was reverse-transcribed by using the Easyscript First-Strand cDNA synthesis Supermix (Transgen, AE301) according to the manufacturer's instructions. Relative mRNA expression was analyzed by using SYBR green qPCR Master Mix (Vazyme) with the indicated mGluR2, SARS-CoV-2 N, and VSV (Indiana strain) P gene-specific primers. The $2^{-\Delta\Delta Ct}$ method was used to calculate the relative gene expression level, with β-actin (Vero-E6 cells) or 28S rRNA (Caco-2 cells, HPAE cells) as the internal control. The primer sequences of individual genes are listed in Table S1.

Virus infection assays

For HRB25 infection, cells were infected at the indicated time and MOI for 1 h at 37°C. Then washed three times with 2% FBS-containing medium, and 2% FBS-containing medium was added to them. Further studies were then carried out.

Western blot analysis

The supernatant of cell lysates was diluted in denaturing buffer and boiled for 15 min. After denaturing, the samples were loaded to a 4%–12% SDS-PAGE gel (Genscript) and separated by electrophoresis. Proteins were transferred to a PVDF membrane (Merck-Millipore, ISEQ00010). The PVDF membrane was blocked with 5% skim milk in PBS containing 0.1% Tween-20, and then incubated with the primary antibodies: anti-Flag antibody (1:1000, Genscript, A00187), anti-Myc antibody (1:1000, Genscript, A00172), anti-GST antibody (1:1000, Genscript, A00097). Then, the membrane was washed three times with PBS and incubated with HRP-conjugated Goat anti-Mouse antibody (1:10000, Genscript, A00160) and Goat anti-Rabbit antibody (1:10000, Genscript, A00098). After three thorough washes with PBST buffer, target protein bands were detected by using the enhanced chemiluminescence (ECL) reagent (Merck Millipore, WBLUR0500).

Co-immunoprecipitation

mGluR2-Flag and SARS-CoV-2 S-Myc, SARS-CoV-2 S1-Myc, SARS-CoV-2 RBD-Myc, SARS-CoV S-Myc, ACE2-Myc, MERS-CoV S-Myc and DPP4-Myc were respectively co-transfected into HEK293 cells as indicated with TransIT-293 transfection reagent (Mirus, MIR2701) by following the manufacturer's instructions. At 48 h post-transfection, the cells were washed with PBS and lysed with 1% NP-40 buffer (Beyotime, P0013F) containing a protease inhibitor for 1 h at 4°C. Cell lysates were centrifuged (12,000 rpm) for 20 min at 4°C to remove cell debris. Then, supernatant was collected and mixed with 40 μl of protein G

Agarose (Roche, 11243233001) for 4 h at 4°C on a flip shaker. The protein G beads were then removed by centrifugation, and the supernatant was collected and mixed with anti-Flag antibody-conjugated agarose beads (Sigma, A2220) for 6 h at 4°C on a flip shaker. After conjugation, the beads were washed 5 times with pre-chilled 1% NP-40 PBS buffer. Finally, the beads were resuspended in PBS and mixed with protein sample loading buffer, boiled for 15 min, and subjected to SDS-PAGE.

Pull-down assay

For pull-down assays, the N-terminal GST-tagged soluble ectodomain of mGluR2 (mGluR2-GST, amino acids 19–567) was expressed and purified by FriendBio Technology (Wuhan, Hubei, China). The purified GST-tagged proteins were incubated with Glutathione Sepharose 4B beads (GE Healthcare Bio-science, 17-0756-01) at 4ºC for 2 h. The beads were then washed and incubated with whole cell lysates from HEK293 cells expressing Myc-tagged proteins at 4ºC for 5 h with constant rotation. After conjugation, the beads were washed five times with wash buffer (pH 8.5, 20 mM Tris, 500 mM NaCl, 2 mM EDTA) and re-suspended in PBS and protein sample loading buffer. The samples were then subjected to SDS-PAGE, and assessed by western blot analysis.

Cell viability assay

Cell viability was determined by using the Cell Titer-Glo kit (Promega, G9242). Cells were seeded onto 96-well plates with opaque walls. Antibody at the indicated concentrations was added, and 48 h later, Cell Titer-Glo reagent was added to each well. Luminescence was measured with a GloMax 96 Microplate Luminometer (Promega).

Antibody blocking assay

Vero-E6 cells or Caco-2 cells were seeded onto 96-well plates. Cells were treated with the indicated concentrations of mGluR2 antibody (Santa Cruz Biotechnology, sc-271654), or isotype antibody (Southern Biotech, 0103-01) for 1 h on ice. Vero-E6 cells and Caco-2 cells were infected with HRB25 at MOI of 0.002 and 0.02, respectively, for 1 h at 4°C in presence of the indicated concentrations of antibody, then washed, and incubated with medium containing antibody at 37ºC. At 48 h p.i., the culture supernatant was harvested to assess virus titers by plaque forming assay.

HPAE cells were seeded onto 48-well plates for 72 h, then treated with mGluR2 antibody (15 μg/mL) or isotype antibody (15 μg/mL), and infected with HRB25 (MOI=0.01) as described above. At 48 h p.i. the viral RNA expression level relative to 28S rRNA was calculated by qPCR.

Vero-E6 cells were treated with the indicated concentrations of mGluR2 antibody, or isotype antibody, then infected with VSV (MOI=0.005), rVSV-SARS-CoV-S (MOI=0.05) or rVSV-MERS-CoV-S (MOI=0.05) as described above. The infection culture supernatant of VSV was harvested at 24 h p.i..

Soluble mGluR2 ectodomain neutralization assay

Vero-E6 cells were seeded onto 24-well plates. HRB25 at an MOI of 0.0002 was mixed with purified the N-terminal GST-tagged soluble ectodomain of mGluR2 at different concentrations or with GST in 100 μl of cell culture medium at 4ºC for 1 h [17]. Cells were then incubated with the virus-protein mix at 37ºC for 1 h, then washed and incubated with growth medium. At 24 h p.i., the culture supernatant was harvested to assess virus titers by using a plaque forming assay.

Viral binding assay

Cell-bound HRB25, rVSV-SARS-CoV-S, or rVSV-MERS-CoV-S was assessed by qPCR. Cells were transfected with the indicated siRNA for 72 h, then the cells were transferred onto ice for 20 min. Then, HRB25 (MOI=10), rVSV-SARS-CoV-S (MOI=10), or rVSV-MERS-CoV-S (MOI=10) was added to the cells at 4°C for 1 h. Unbound virions were removed by three washes with pre-chilled PBS, and the cells were then lysed by TRIZOL. The viral RNA expression level relative to β-actin (Vero-E6 cells) or 28S rRNA (Caco-2 cells) was then calculated by use of qPCR.

Viral internalization assay

Internalized virions were detected by qPCR. Cells were transfected with the indicated siRNA for 72 h and then were transferred onto ice for 20 min. HRB25 (MOI=10), rVSV-SARS-CoV-S (MOI=10), or rVSV-MERS-CoV-S (MOI=10) was then added to cells at 4°C for 1 h. After removal of the unbound virions by extensive washing with chilled PBS, the cells were moved to 37ºC for 1 h to allow endocytosis. After 1 h, the cells were washed three times for 3 min with acidic buffer (50 mM glycine, 100 mM NaCl, pH 3.0), then trypsinized to remove HRB25, rVSV-SARS-CoV-S, or rVSV-MERS-CoV-S bound to the cell surface. The cells were lysed for total RNA extraction and followed by RT-qPCR to detect internalized viruses.

For microscopy, Vero-E6 cells were transfected with the indicated siRNA and cultured on Millicell EZ slide 4-Well Glass (Merck Millipore, PEZGS0416) for 72 h. After HRB25 internalization 1 h at 37ºC, the cells were immediately fixed with 3% paraformaldehyde for 15 min at room temperature. If needed, they were permeabilized with 0.1% Triton X-100 in PBS for 10 min at room temperature and then incubated with 1% BSA for 30 min to block nonspecific binding of antibodies. Both permeabilized and unpermeabilized cells were incubated with anti-SARS-CoV-2 S protein rabbit monoclonal antibody (1:100, Sino Biologicals, 40150-R007) overnight at 4°C, then washed and stained with goat anti-rabbit Alexa Fluor 488 (1:1000, Thermo Fisher, A11034) for 1 h. Nuclei were visualized by staining with Hoechst 33342, and coverslips were mounted in Fluoroshield™ histology mounting medium (Sigma, F6182) onto slides. Fluorescence intensity was quantified with a Zeiss LSM880 laser-scanning confocal microscope (Carl Zeiss AG) equipped with Airyscan (Plan-Apochromat, objective 63×, 1.4 Numerical Aperture DIC oil immersion objective) by using ZEN software. The resolution of the acquired images was 1024×1024. The cell-bound HRB25 signal intensities from at least 110 cells per sample were quantified by using ZEN software.

Multiplex immunofluorescence

Cells were cultured on Millicell EZ slide 4-Well Glass, then infected with HRB25 (MOI=10) at 37ºC for 5 min. Then, the cells were thoroughly washed with PBS and fixed with 3% paraformaldehyde. Multiplex immunofluorescence with Tyramide Signal Amplification (TSA) was performed by following the previously established protocol [17]. Briefly, endogenous peroxidase activity was quenched. After permeabilization with 0.1% Triton X-100 and blocking steps (Zsbio, ZLI-9056), the samples were incubated with primary antibodies followed by HRP-conjugated secondary antibodies. Multiplex fluorescence labeling was performed using TSA-dendron-fluorophores (NEON 7-color Allround Discovery Kit for FFPE, Histova Biotechnology, NEFP750). A commercial antibody stripping buffer was employed to remove the primary and secondary antibodies while retaining the TSA signal by incubation for 30 min at 37ºC. After a brief rinse, other antigens were serially detected by using spectrally different TSA reagents and following the above method. The primary antibodies used in this study were: ACE2 (1:400, Abcam, ab108252), SARS-CoV-2 nucleocapsid protein (1:1000, Sinobiological, 40143-R004), mGluR2 (1:200, Santa Cruz Biotechnology, sc-271654), and clathrin (1:400, CST, 4796S). The secondary antibodies were HRP-conjugated anti-rabbit IgG (Zsbio, PV-6001) and HRP-conjugated anti-mouse IgG (Zsbio, PV-6002). Images were acquired using a Zeiss LSM880 laser-scanning confocal microscope equipped with Airyscan. The resolution of the acquired images was 2048 × 2048.

Multiplex immunofluorescence staining for detection of SARS-CoV-2 targeted cells in olfactory epithelium and lung sections of mouse were conducted. 4-μm-thick paraffin sections were deparaffinized in xylene and rehydrated in a series of graded alcohols. Antigen retrievals were performed in citrate buffer (pH=6) with a microwave oven for 20 min at 95°C followed by a 20 min cool down at room temperature. Multiplex fluorescence labeling was performed using TSA-dendron-fluorophores (NEON 7-color Allround Discovery Kit for FFPE, Histova Biotechnology, NEFP750). Briefly, primary antibody was incubated for 2-4 h in a humidified chamber at 37°C, followed by detection using the HRP-conjugated secondary antibody and TSA-dendron-fluorophores. Afterwards, the primary and secondary antibodies were thoroughly eliminated by heating the slides in retrieval/elution buffer (Abcracker, Histova Biotechnology, ABCFR5L) for 10 s at 95°C using microwave. In a serial fashion, each antigen was labeled by distinct fluorophores. The multiplex immunofluorescence staining of normal human (male, 21-year-old) lung section, which was obtained from Shanghai Biochip Company, China, was performed as above.

Multiplex antibody panels applied in this study include: mGluR2 (1:400, Abcam, ab150387), Ace2 (1:400, Abcam, ab108252), SARS-CoV-2 nucleocapsid protein (1:1000, Sinobiological, 40143-R004), GAP43 (1:1000, Abcam, ab75810), OMP (1:1500, Abcam, ab183947), CK5 (1:800, Abcam, ab52635), CK8 (1:800, Abcam, ab53280), CC10 (1:500, Millipore, 07-623), Foxj1 (1:1000, Abcam, ab235445), SPC (1:500, Abcam, ab211326), Tubb4 (1:1000, Abcam, ab179504). After all the antibodies were detected sequentially, the slices were imaged using the confocal laser scanning microscopy platform Zeiss LSM880.

Genotypic identification

The genotype of the mice was identified by using a PCR assay. Tail tissues were obtained

from 6-week-old mice and whole genome DNA was extracted with the TIANamp Genomic DNA Kit (TIANGEN DP304-03) by following the manufacturer's instructions. WT mGluR2 was identified with specific primers (forward, 5'- CGTGGCCTGATATCTCTACCGT-3'; reverse, 5'-TGTCCACAGTGTGGTGCTGAAT-3) and mGluR2 $^{-/-}$ was identified with specific primers (forward, 5'- CGTGGCCTGATATCTCTACCGT-3'; reverse, 5'-ACCGTCTCCTAGAAGAGTGGACA-3); 2 X Taq reaction component (Vazyme, P112-03) was used in the reaction. The conditions for PCR were as follows: one cycle of 95 °C for 5 min, 20 cycles of 98 °C for 30 s, 65 °C for 30 s and drop 0.5 ° C per cycle, 72 °C for 45 s, 20 cycles of 98 °C for 30 s, 55 °C for 30 s, 72 °C for 45 s, and one cycle of 72 °C for 5 min.

Animal experiments

Wild-type and mGluR2$^{-/-}$ mice were inoculated intranasally with the indicated PFU of HRB26M in a volume of 50 μl. At 3 days p.i., all mice in each group were euthanized and their nasal turbinates and lungs were collected to detect viral RNA and infectious viruses. Viral RNA copies and infectious titers were detected by qPCR and plaque assays, respectively.

References

1 Zhou, P. *et al.* Addendum: A pneumonia outbreak associated with a new coronavirus of probable bat origin. *Nature* **588**, E6, doi:10.1038/s41586-020-2951-z (2020).

2 Bayati, A., Kumar, R., Francis, V. & McPherson, P. S. SARS-CoV-2 infects cells following viral entry via clathrin-mediated endocytosis. *J Biol Chem*, 100306, doi:10.1016/j.jbc.2021.100306 (2021).

3 Hoffmann, M. *et al.* SARS-CoV-2 Cell Entry Depends on ACE2 and TMPRSS2 and Is Blocked by a Clinically Proven Protease Inhibitor. *Cell* **181**, 271-280 e278, doi:10.1016/j.cell.2020.02.052 (2020).

4 Letko, M., Marzi, A. & Munster, V. Functional assessment of cell entry and receptor usage for SARS-CoV-2 and other lineage B betacoronaviruses. *Nat Microbiol* **5**, 562-569, doi:10.1038/s41564-020-0688-y (2020).

5 Coronaviridae Study Group of the International Committee on Taxonomy of, V. The species Severe acute respiratory syndrome-related coronavirus: classifying 2019-nCoV and naming it SARS-CoV-2. *Nat Microbiol* **5**, 536-544, doi:10.1038/s41564-020-0695-z (2020).

6 V'Kovski, P., Kratzel, A., Steiner, S., Stalder, H. & Thiel, V. Coronavirus biology and replication: implications for SARS-CoV-2. *Nat Rev Microbiol*, doi:10.1038/s41579-020-00468-6 (2020).

7 Walls, A. C. *et al.* Structure, Function, and Antigenicity of the SARS-CoV-2 Spike Glycoprotein. *Cell* **181**, 281-292 e286, doi:10.1016/j.cell.2020.02.058 (2020).

8 Cantuti-Castelvetri, L. *et al.* Neuropilin-1 facilitates SARS-CoV-2 cell entry and infectivity. *Science* **370**, 856-860, doi:10.1126/science.abd2985 (2020).

9 Daly, J. L. *et al.* Neuropilin-1 is a host factor for SARS-CoV-2 infection. *Science* **370**, 861-+, doi:10.1126/science.abd3072 (2020).

10 Wang, S. *et al.* AXL is a candidate receptor for SARS-CoV-2 that promotes infection

of pulmonary and bronchial epithelial cells. *Cell Res*, doi:10.1038/s41422-020-00460-y (2021).

11 Clausen, T. M. *et al.* SARS-CoV-2 Infection Depends on Cellular Heparan Sulfate and ACE2. *Cell*, doi:10.1016/j.cell.2020.09.033 (2020).

12 Wei, C. *et al.* HDL-scavenger receptor B type 1 facilitates SARS-CoV-2 entry. *Nat Metab* **2**, 1391-1400, doi:10.1038/s42255-020-00324-0 (2020).

13 Niswender, C. M. & Conn, P. J. Metabotropic glutamate receptors: physiology, pharmacology, and disease. *Annu Rev Pharmacol Toxicol* **50**, 295-322, doi:10.1146/annurev.pharmtox.011008.145533 (2010).

14 Conn, P. J., Lindsley, C. W. & Jones, C. K. Activation of metabotropic glutamate receptors as a novel approach for the treatment of schizophrenia. *Trends Pharmacol Sci* **30**, 25-31, doi:10.1016/j.tips.2008.10.006 (2009).

15 Kalivas, P. W. The glutamate homeostasis hypothesis of addiction. *Nat Rev Neurosci* **10**, 561-572, doi:10.1038/nrn2515 (2009).

16 Conn, P. J. & Pin, J. P. Pharmacology and functions of metabotropic glutamate receptors. *Annu Rev Pharmacol Toxicol* **37**, 205-237, doi:10.1146/annurev.pharmtox.37.1.205 (1997).

17 Wang, J. *et al.* Metabotropic glutamate receptor subtype 2 is a cellular receptor for rabies virus. *Plos Pathog* **14**, e1007189, doi:10.1371/journal.ppat.1007189 (2018).

18 Ohishi, H., Shigemoto, R., Nakanishi, S. & Mizuno, N. Distribution of the messenger RNA for a metabotropic glutamate receptor, mGluR2, in the central nervous system of the rat. *Neuroscience* **53**, 1009-1018, doi:10.1016/0306-4522(93)90485-x (1993).

19 Wang, J. L. *et al.* Mouse-adapted SARS-CoV-2 replicates efficiently in the upper and lower respiratory tract of BALB/c and C57BL/6J mice. *Protein & Cell* **11**, 776-782, doi:10.1007/s13238-020-00767-x (2020).

20 Raj, V. S. *et al.* Dipeptidyl peptidase 4 is a functional receptor for the emerging human coronavirus-EMC. *Nature* **495**, 251-254, doi:10.1038/nature12005 (2013).

21 Liu, R. *et al.* A recombinant VSV-vectored MERS-CoV vaccine induces neutralizing antibody and T cell responses in rhesus monkeys after single dose immunization. *Antiviral Res* **150**, 30-38, doi:10.1016/j.antiviral.2017.12.007 (2018).

22 Zubair, A. S. *et al.* Neuropathogenesis and Neurologic Manifestations of the Coronaviruses in the Age of Coronavirus Disease 2019: A Review. *JAMA Neurol* **77**, 1018-1027, doi:10.1001/jamaneurol.2020.2065 (2020).

23 Arabi, Y. M. *et al.* Severe neurologic syndrome associated with Middle East respiratory syndrome corona virus (MERS-CoV). *Infection* **43**, 495-501, doi:10.1007/s15010-015-0720-y (2015).

24 Huang, C. *et al.* Clinical features of patients infected with 2019 novel coronavirus in Wuhan, China. *Lancet* **395**, 497-506, doi:10.1016/S0140-6736(20)30183-5 (2020).

25 Conde Cardona, G., Quintana Pajaro, L. D., Quintero Marzola, I. D., Ramos Villegas, Y. & Moscote Salazar, L. R. Neurotropism of SARS-CoV 2: Mechanisms and manifestations. *J Neurol Sci* **412**, 116824, doi:10.1016/j.jns.2020.116824 (2020).

26 Song, E. *et al.* Neuroinvasion of SARS-CoV-2 in human and mouse brain. *J Exp Med* **218**, doi:10.1084/jem.20202135 (2021).

27 Meinhardt, J. *et al.* Olfactory transmucosal SARS-CoV-2 invasion as a port of central

nervous system entry in individuals with COVID-19. *Nature Neuroscience*, doi:10.1038/s41593-020-00758-5 (2020).

28 Shi, J. *et al.* Susceptibility of ferrets, cats, dogs, and other domesticated animals to SARS-coronavirus 2. *Science* **368**, 1016-1020, doi:10.1126/science.abb7015 (2020).

Acknowledgments

This work was supported by the National Key R&D Program of China (2018YFC1200601, 2020YFC0846500).

Contributions

ZG. B. designed the study. JL. W., XX. W., ZY. W., G. Y., J. L., QQ. H., L. S., RQ. L., ZR. S., XJ. H., X. Y., GX. Z., C. W., WY. C., XJ. W., and JY. G. performed the experiments. JL. W. and ZG. B. analyzed the data. JL. W. and ZG. B. wrote the paper. JL. W., and G. Y., XX. W. contributed equally to this work. ZG. B supervised the whole project.

Competing interests

The authors declare no competing interests.

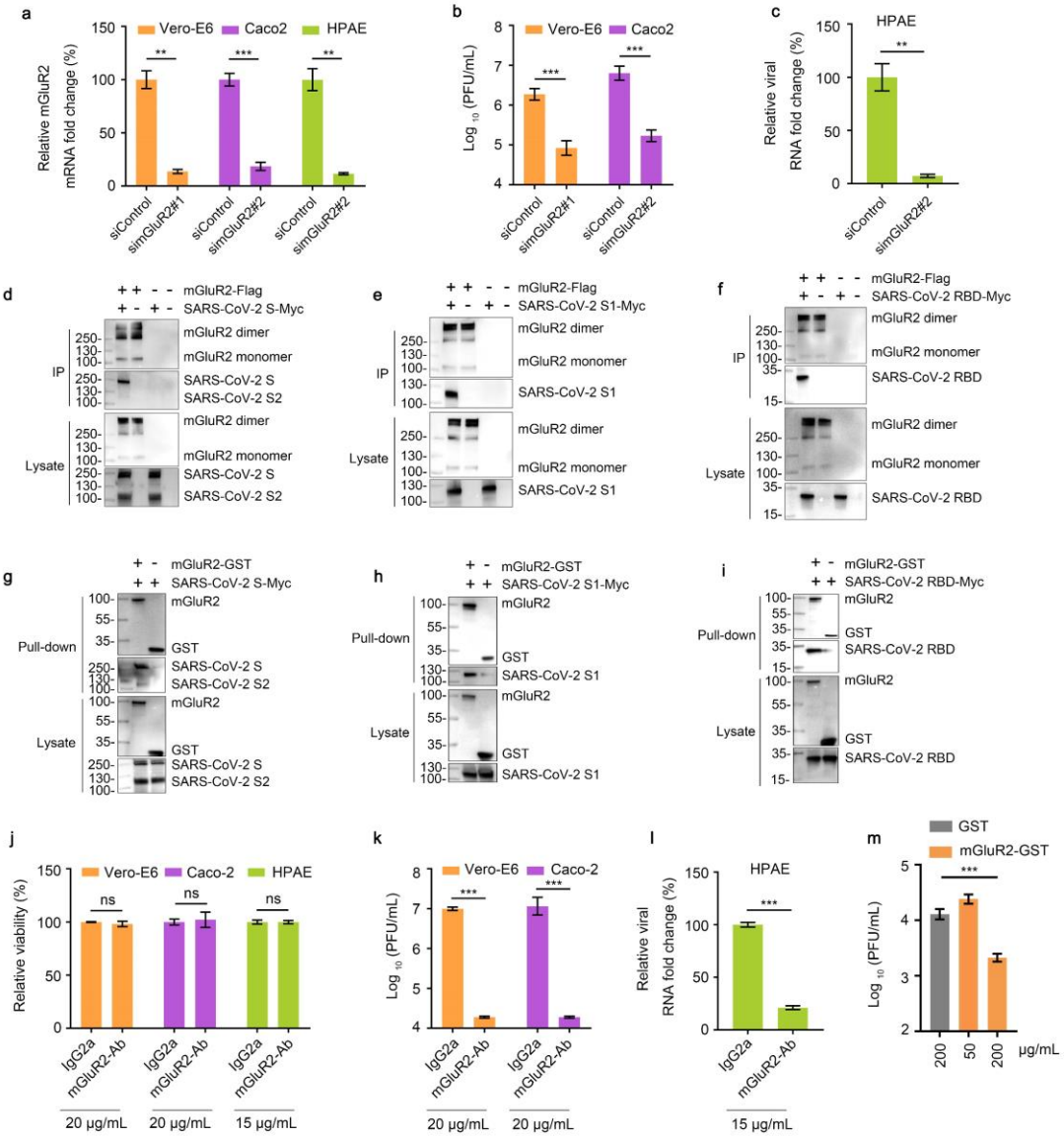

Fig. 1: mGluR2 is a receptor for SARS-CoV-2 infection. a, Knockdown of mGluR2 was measured by qPCR in Vero-E6 cells, Caco-2 cells and HPAE cells (**a**). simGluR2#1, simGluR2#2, an siRNA specific for mGluR2 mRNA from monkey and human, respectively, siControl, scrambled RNA. **b and c**, mGluR2-silenced Vero-E6 cells (**b**), Caco-2 cells (**b**) or HPAE cells (**c**) were infected with HRB25 (MOI=0.01 for Vero-E6 cells; MOI=0.05 for Caco-2 cells; MOI=0.001 for HPAE cells). At 24 h p.i., the culture supernatant was detected by plaque assays or qPCR. **d-f**, mGluR2-Flag and SARS-CoV-2 S-Myc (**d**), SARS-CoV-2 S1-Myc (**e**) or SARS-CoV-2 RBD-Myc (**f**) were co-transfected in HEK293 cells and then immunoprecipitated by using anti-Flag agarose beads. **g-i**, Purified recombinant GST-tagged mGluR2 ectodomain (mGluR2-GST) was pooled with lysate from SARS-CoV-2 S-Myc- (**g**), SARS-CoV-2 S1-Myc- (**h**) or SARS-CoV-2 RBD-Myc- (**i**) transfected HEK293 cells and then pull-down was performed using anti-GST beads. **j**, Cell viability was determined by using a commercial cell viability assay kit. **k and l**, Vero-E6 cells, Caco-2 cells and HPAE cells were

635 treated with mGluR2-Ab at different concentrations or IgG2a (20 μg/mL for Vero-E6 cells
636 and Caco-2 cells, 15 μg/mL for HPAE cells) for 1 h at 4°C, then infected with HRB25
637 (MOI=0.002 for Vero-E6 cells; MOI=0.02 for Caco-2 cells; MOI=0.01 for HPAE cells). The
638 culture supernatant was detected by plaque assays or qPCR at 48 h p.i.. **m**, HRB25
639 (MOI=0.0002) was pooled with different concentrations of mGluR2-GST or GST (200
640 μg/mL), then Vero-E6 cells were infected by mixing for 1 h at 37°C. The culture supernatant
641 was detected by plaque assays at 24 h p.i..
642 n=3, mean ± SD, Student's test, ns, not significant, $^{**}p < 0.01$, $^{***}p < 0.001$.
643

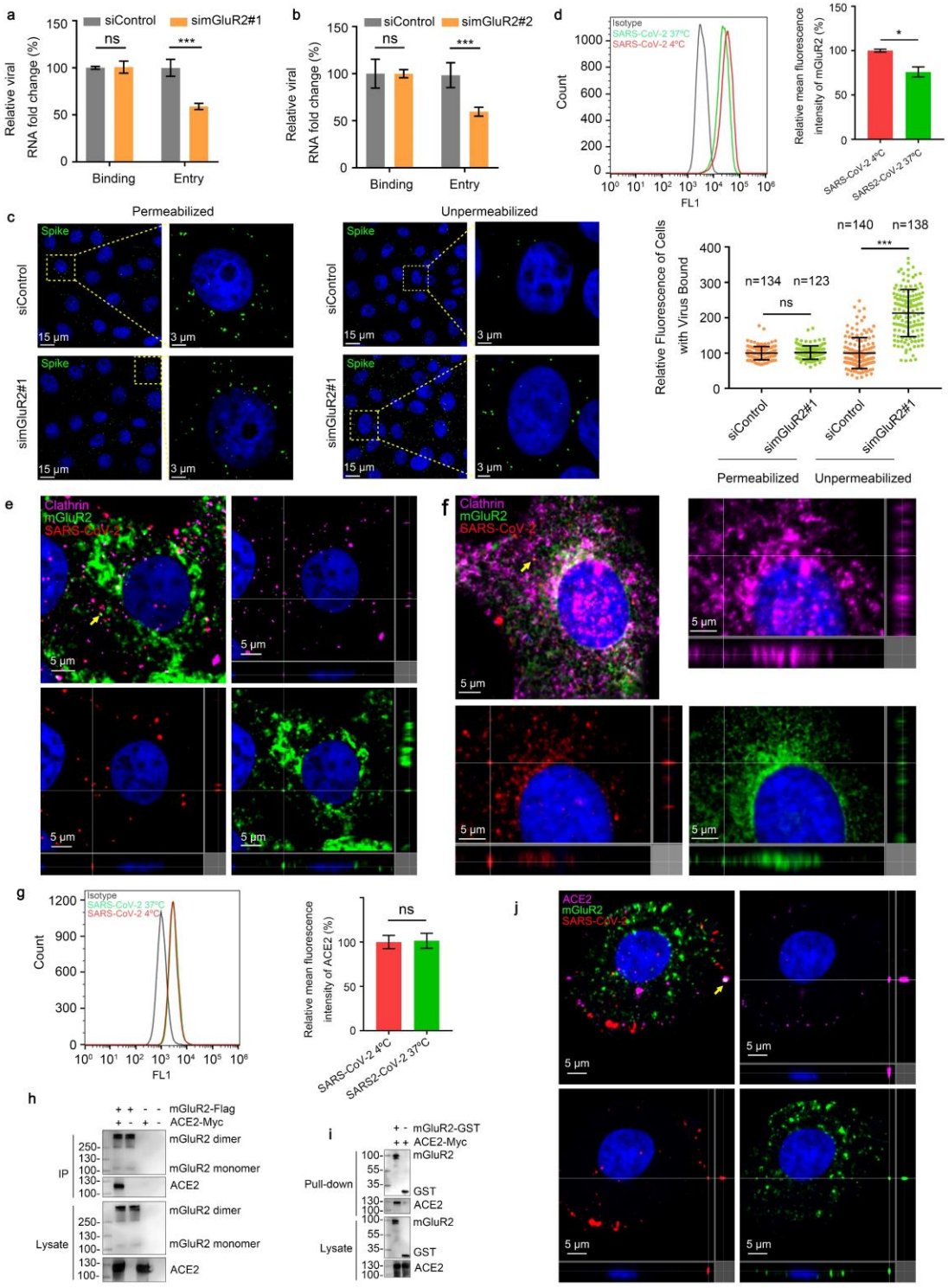

Fig. 2: mGluR2 is required for endocytosis of SARS-CoV-2 but not for cell binding. a and b, SARS-CoV-2 binding and internalization assays were performed in mGluR2-silenced Vero-E6 cells (**a**) and Caco-2 cells (**b**). **c**, Vero-E6 cells were treated as described in (a), except they were not treated with acid buffer/trypsin. Cell nuclei (blue), SARS-CoV-2 S protein (green). Representative images are shown. The signal intensities of cell-bound HRB25 in each sample were quantified. The dashed box is magnified at the indicated location of the same image. The circles represent individual data points. n, the number of quantified cells. **d and g**, The surface expression level of mGluR2 (**d**) and ACE2 (**g**) were detected by flow

cytometry after infection with HRB25 (MOI=5) at 37°C for 30 min under unpermeabilized conditions in Vero-E6 cells. **e and f**, Multiplex immunofluorescence was performed in Vero-E6 cells (MOI=50) (**e**) and HPAE cells (MOI=10) (**f**). The yellow arrowhead indicates the representative colocalization of mGluR2 (green), SARS-CoV-2 N protein (red), and clathrin (purple), shown in three dimensions. **h**, HEK293 cells were co-transfected with mGluR2-Flag and ACE2-Myc. Cell lysates were immunoprecipitated by using anti-Flag agarose beads. **i**, mGluR2-GST was pooled with lysate from ACE2-Myc-transfected HEK293 cells and then pull-down was performed using anti-GST beads. **j**, As described in (e). The yellow arrowhead indicates representative colocalization of mGluR2 (green), the SARS-CoV-2 N protein (red), and ACE2 (purple), shown in three dimensions.
n=3, mean ± SD, Student's test, ns, not significant, *$p < 0.05$, ***$p < 0.001$

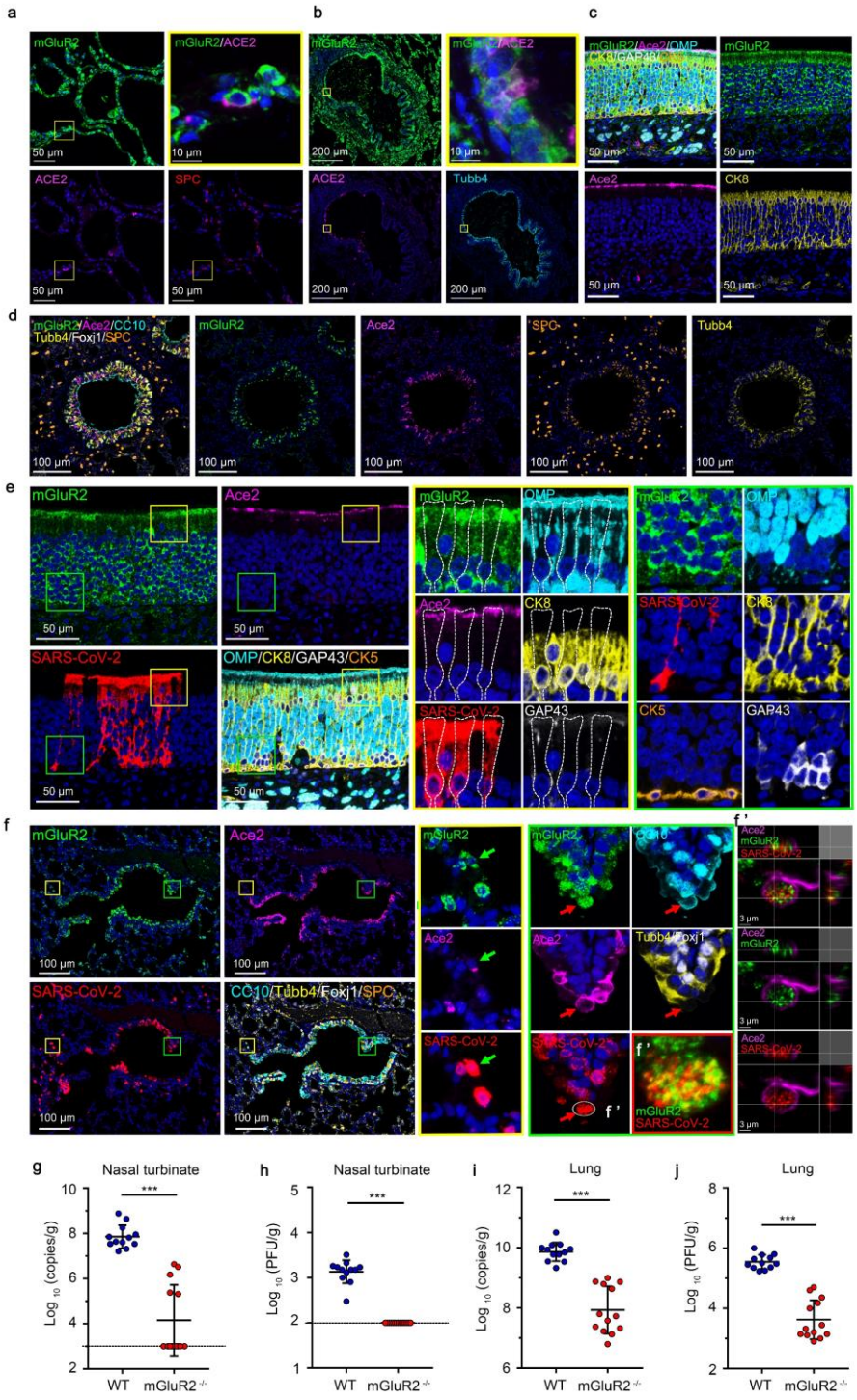

Fig. 3: mGluR2 is required for SARS-CoV-2 infection of mice. a and b, Multiplex immunofluorescence staining for detection of mGluR2 positive cells in normal human lung section. mGluR2 (green), ACE2 (magenta), Tubb4 (cyan), SPC (red). The yellow areas are shown adjacently at a higher magnification in alveoli (**a**) or bronchia (**b**). **c and e**, Multiplex immunofluorescence staining for detection of mGluR2 positive cells in olfactory epithelium sections of young mouse uninfected (**c**) or infected (**e**) by SARS-CoV-2 on day 3 p.i.. SARS-CoV-2 N protein (red), mGluR2 (green), Ace2 (magenta), GAP43 (white), CK5 (gold), CK8 (yellow), OMP (cyan). The yellow and green areas are shown adjacently at a higher

magnification, respectively. The dash box indicates the individual cell boundary. **d and f**, Multiplex immunofluorescence staining for detection of mGluR2 positive cells in lung sections of young mouse uninfected (**d**) or infected (**f**) by SARS-CoV-2 on day 3 p.i.. SARS-CoV-2 N protein (red), mGluR2 (green), Ace2 (magenta), Foxj1 (white), SPC (gold), Tubb4 (yellow), CC10 (cyan). The yellow and green areas are shown adjacently at a higher magnification, respectively. Red arrowhead indicates $mGluR2^{+}/SARS\text{-}CoV\text{-}2^{+}/Ace2^{+}/CC10^{+}$ cell, and green arrowhead indicates $mGluR2^{+}/SARS\text{-}CoV\text{-}2^{+}/Ace2^{+}$ cell. **f'**, the 3D-rendered image was generated by using Imaris software and the co-localization of mGluR2 and SARS-CoV-2 form the two single fluorescence channels is showed. **g-j**, mGluR2 gene knockout ($mGluR2^{-/-}$) (n=13) and wild-type (WT) (n=12) mice were infected with HRB26M (150 PFU/mouse), a mouse-adapted SARS-CoV-2 strain, via intranasal inoculation. At 3-days p.i., viral RNA copies and virus titers in the nasal turbinates (**g and h**) and lungs (**i and j**) were determined by qPCR (**g and i**) and plaque assays (**h and j**), respectively. The horizontal dashed line indicates the limit of detection. mean ± SD, Student's test, $***p < 0.001$.

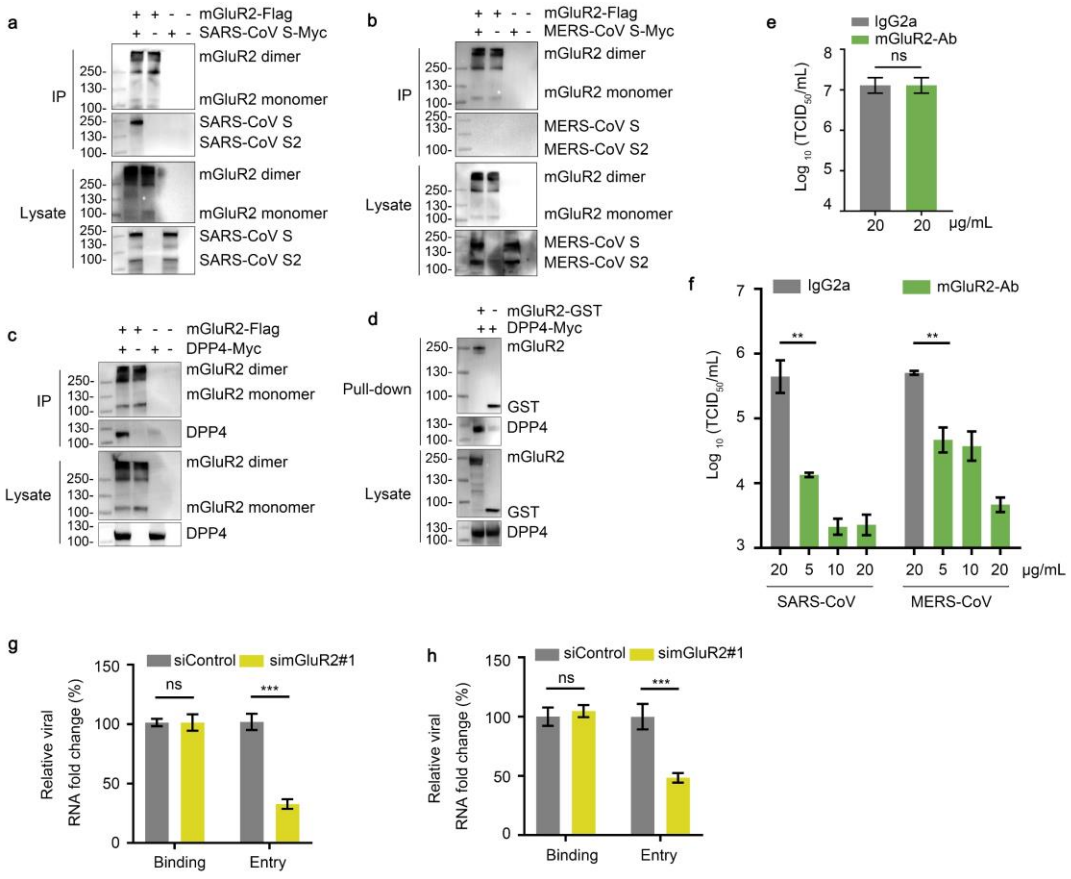

Figure 4. mGluR2 is important for both SARS-CoV S- and MERS-CoV-2 S-mediated endocytosis. a-c, mGluR2-Flag and SARS-CoV S-Myc (**a**), MERS-CoV S-Myc (**b**) or DPP4-Myc (**c**) were co-transfected in HEK293 cells, and were then immunoprecipitated by using anti-Flag agarose beads. **d**, mGluR2-GST was pooled with lysate from DPP4-Myc-transfected HEK293 cells and then pull-downed by using anti-GST beads. **e and f**, Vero-E6 cells were treated with mGluR2-Ab, or IgG2a (20 μg/mL) for 1 h at 4°C, then infected with VSV (MOI=0.005) (**e**), rVSV-SARS-CoV-S (MOI=0.05) or rVSV-MERS-CoV-S (MOI=0.05) (**f**) for 1 h at 4°C. The culture supernatant was detected by $TCID_{50}$ assays at 24 h p.i.. **g and h**, Viral binding and internalization assays were performed in mGluR2-silenced Vero-E6 cells. Cells were incubated with rVSV-SARS-CoV-S (MOI=10) (**g**) or rVSV-MERS-CoV-S (MOI=10) (**h**), respectively.
n=3, mean ± SD, Student's test, ns, not significant, $^{**}p < 0.01$, $^{***}p < 0.001$.

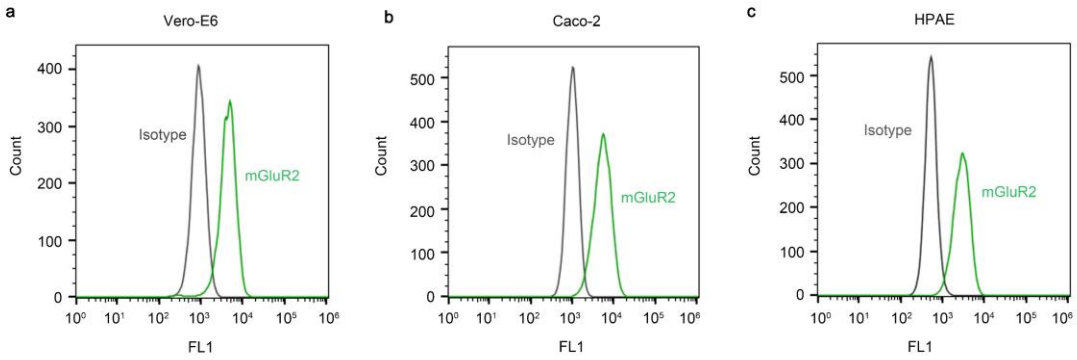

703

704 **Extended Data Figure 1. Expression of mGluR2 on Vero-E6 cells, Caco-2 cells, and**
705 **HPAE cells. a-c**, Surface expression of mGluR2 on Vero-E6 cells (**a**), Caco-2 cells (**b**) and
706 HPAE cells (**c**) were confirmed by flow cytometry.

707

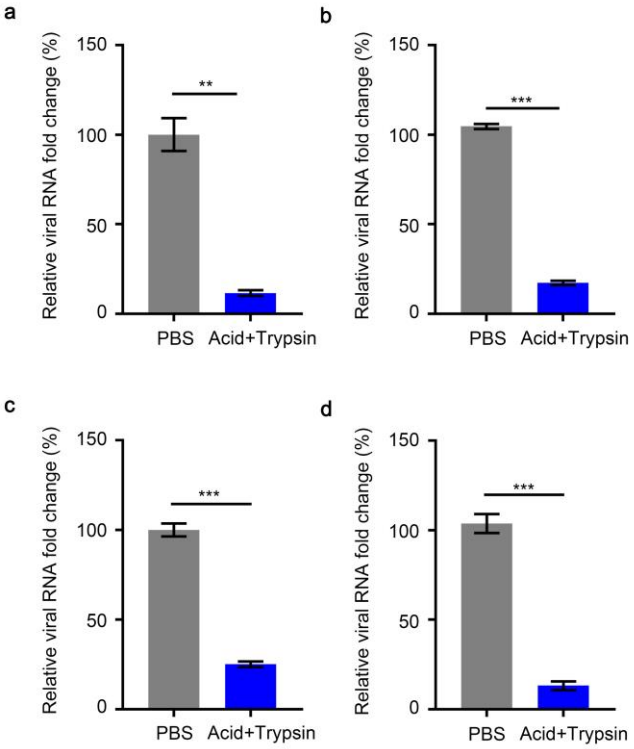

Extended Data Figure 2. Cells treated with acid buffer/trypsin could efficiently remove bound SARS-CoV-2, rVSV-SARS-CoV-S, or rVSV-MERS-CoV-S

a and b, Vero-E6 cells (**a**) and Caco-2 cells (**b**) were incubated with HRB25 (MOI=10) for 1 h at 4°C and washed to remove unbound virus. The cells were washed with acid buffer/trypsin and lysed for qPCR to detect SARS-CoV-2 bound to the cell surface. n=3, mean ± SD, Student's test, $^{**}p < 0.01$, $^{***}p < 0.001$. **c and d**, Vero-E6 cells were treated as described in (**a**), but incubated with rVSV-SARS-CoV-S (MOI=10) (**c**) or rVSV-MERS-CoV-S (MOI=10) (**d**). n=3, mean ± SD, Student's test, $^{***}p < 0.001$.

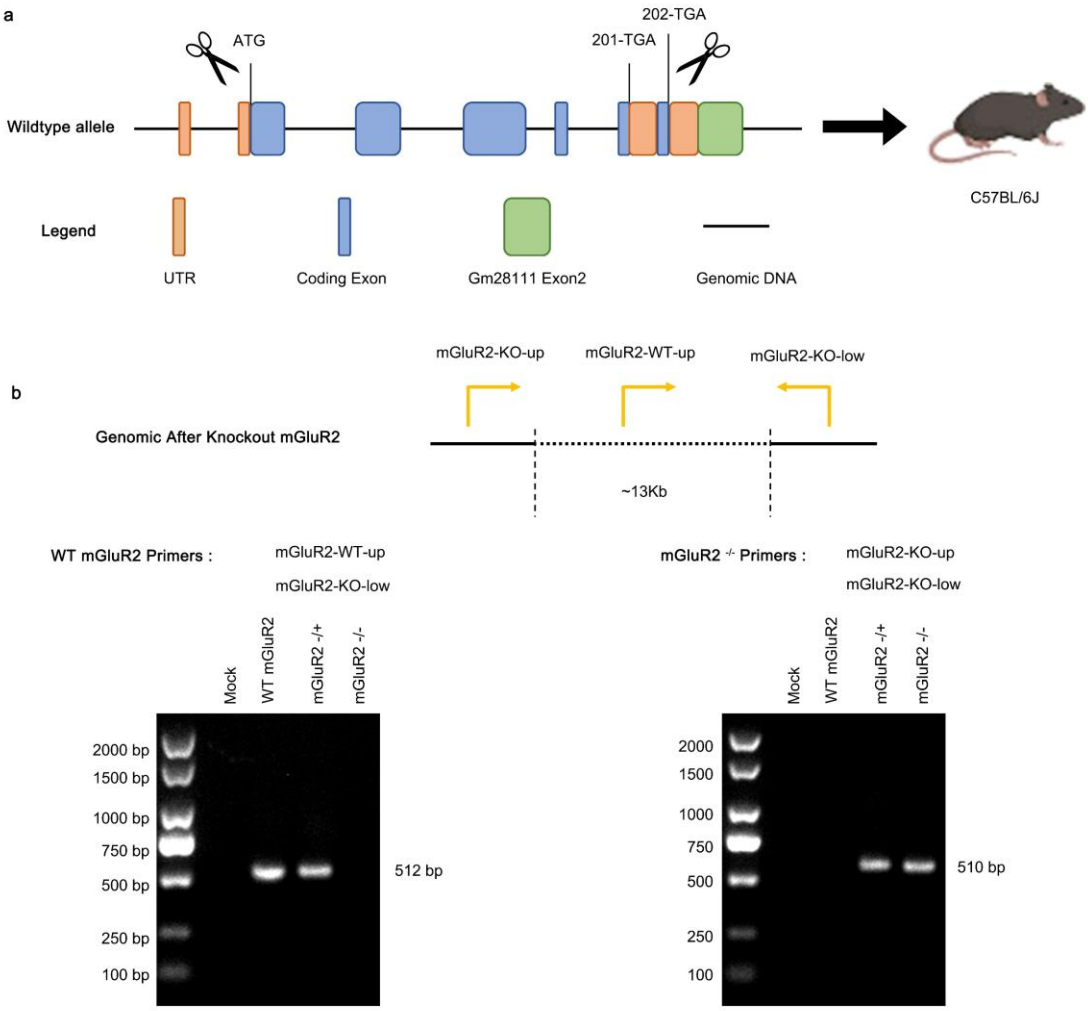

718

719 **Extended Data Figure 3. Generation of mGluR2 gene knockout mouse**

720 **a**, Diagram of the mGluR2 gene deletion. **b**, Genotypic identification with PCR analysis of

721 genomic DNA samples obtained from mouse tails.

722

Supplementary Table 1: Sequences for siRNA, qPCR, mGluR2-sgRNA and mGluR2$^{-/-}$ mice PCR

Genes	Forward	Reverse
simGluR2 #1	CAUUGAGGCCUUUGAGCUAdTdT	UAGCUCAAAGGCCUCAAUGdTdT
simGluR2 #2	CGAUUGGACGAAUUCACUUtt	AAGUGAAUUCGUCCAAUCGgt
mGluR2 (Human)-RT-qPCR	GCACAGGCAAGGAGACAGC	GAGGCAGCCAAGCACCAC
mGluR2 (Green monkey)-RT-qPCR	GCTACAACATCTTCACCTA	CACACTCTTCACCTCATT
SARS-CoV-2 N gene-RT-qPCR	GGGGAACTTCTCCTGCTAGAAT	CAGACATTTTGCTCTCAAGCTG
VSV (Indiana strain) P gene-RT-qPCR	GTGACGGACGAATGTCTCATAA	TTTGACTCTCGCCTGATTGTAC
Beta-actin (Green monkey)-RT-qPCR	GACAGGATGCAGAAGGAGATTAC	CTGCTTGCTGATCCACATCT
28S (Human) rRNA-RT-qPCR	GGGTGGTAAACTCCATCTAAGG	GCCCTCTTGAACTCTCTCTTC
mGluR2-sgRNA 1	CCTCTTACTCCGTGGCATAT	ATATGCCACGGAGTAAGAGG
mGluR2-sgRNA 2	TGGGGATGAGAGCTAACACT	AGTGTTAGCTCTCATCCCCA
mGluR2-sgRNA 3	GCGACCAGATCCCCTAGGTC	GACCTAGGGGATCTGGTCGC
mGluR2-sgRNA 4	TGTAGAGTTTAAGGCTCGCC	GGCGAGCCTTAAACTCTACA
mGluR2-WT	CGTGGCCTGATATCTCTACCGT	TGTCCACAGTGTGGTGCTGAAT
mGluR2-KO	CGTGGCCTGATATCTCTACCGT	ACCGTCTCCTAGAAGAGTGGACA

Extended Data Table 1. Primers sequences

Figures

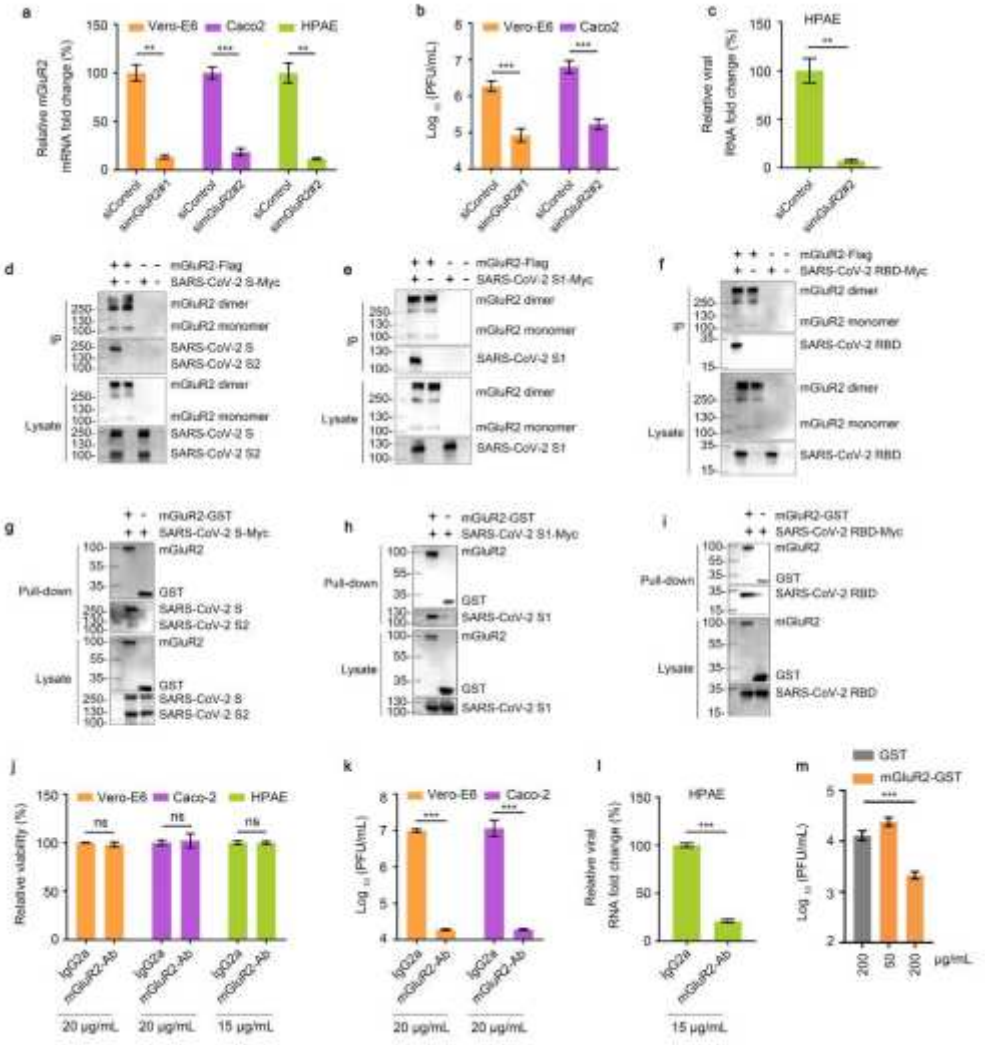

Figure 1

mGluR2 is a receptor for SARS-CoV-2 infection.

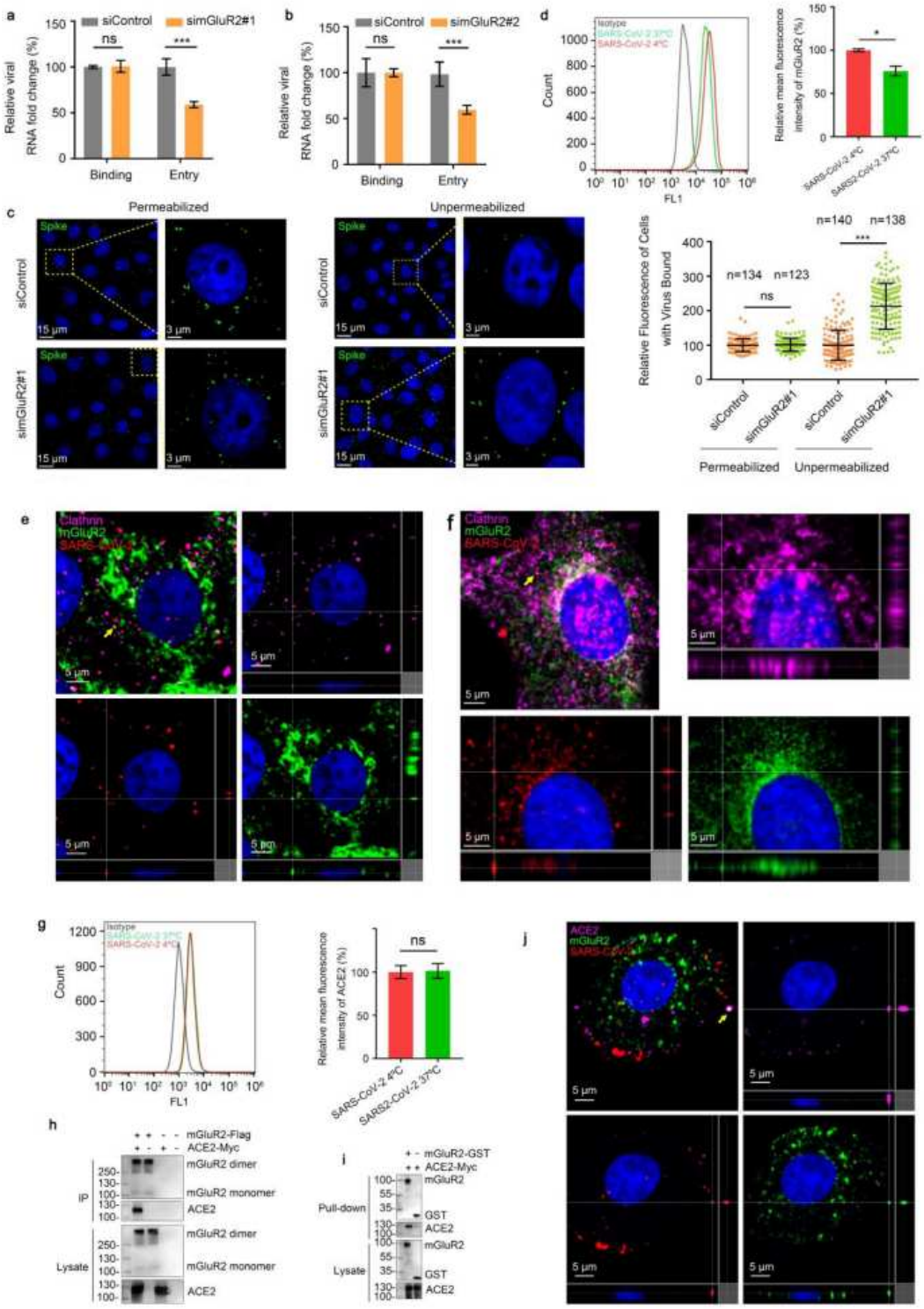

Figure 2

mGluR2 is required for endocytosis of SARS-CoV-2 but not for cell binding.

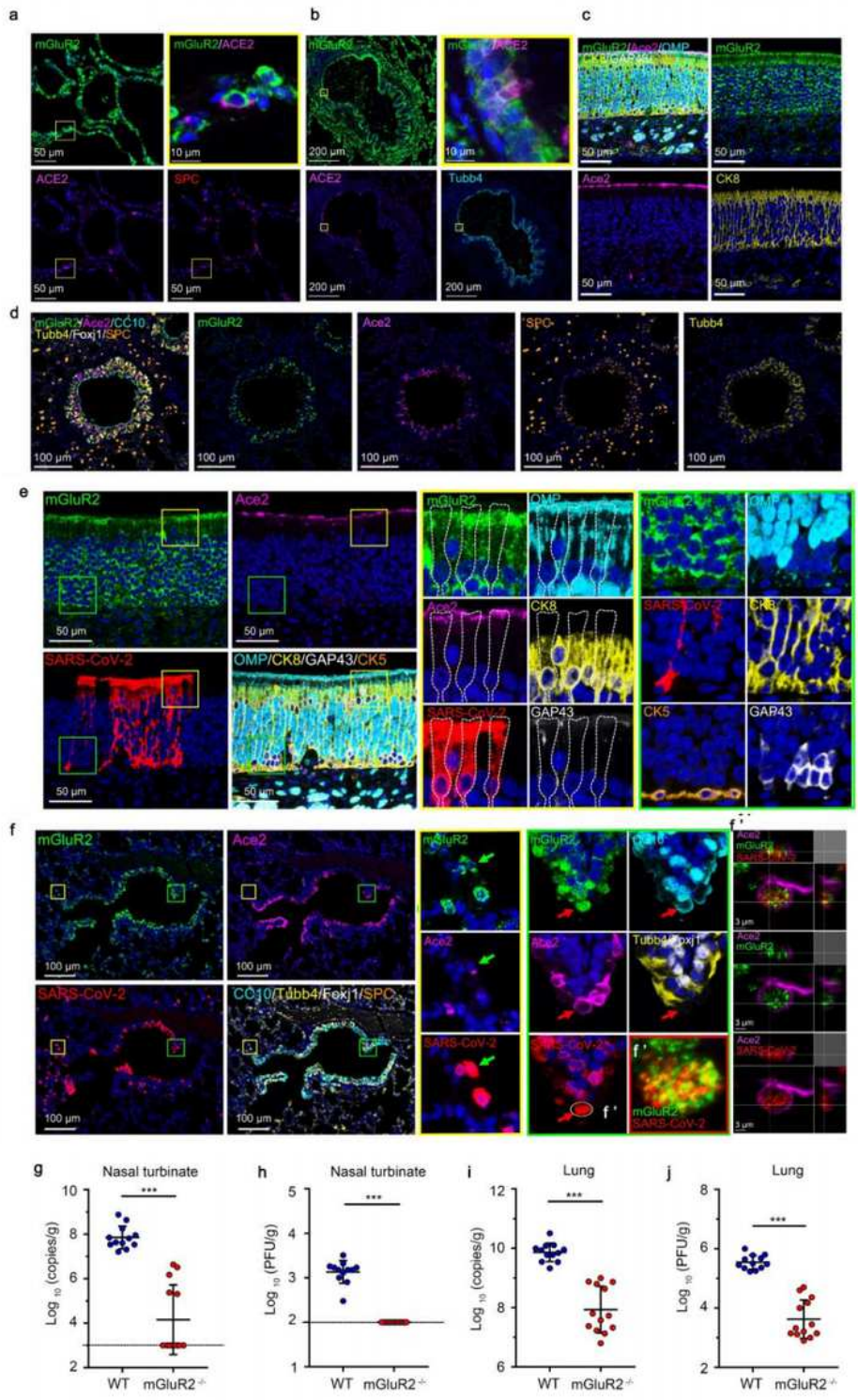

Figure 3

mGluR2 is required for SARS-CoV-2 infection of mice.

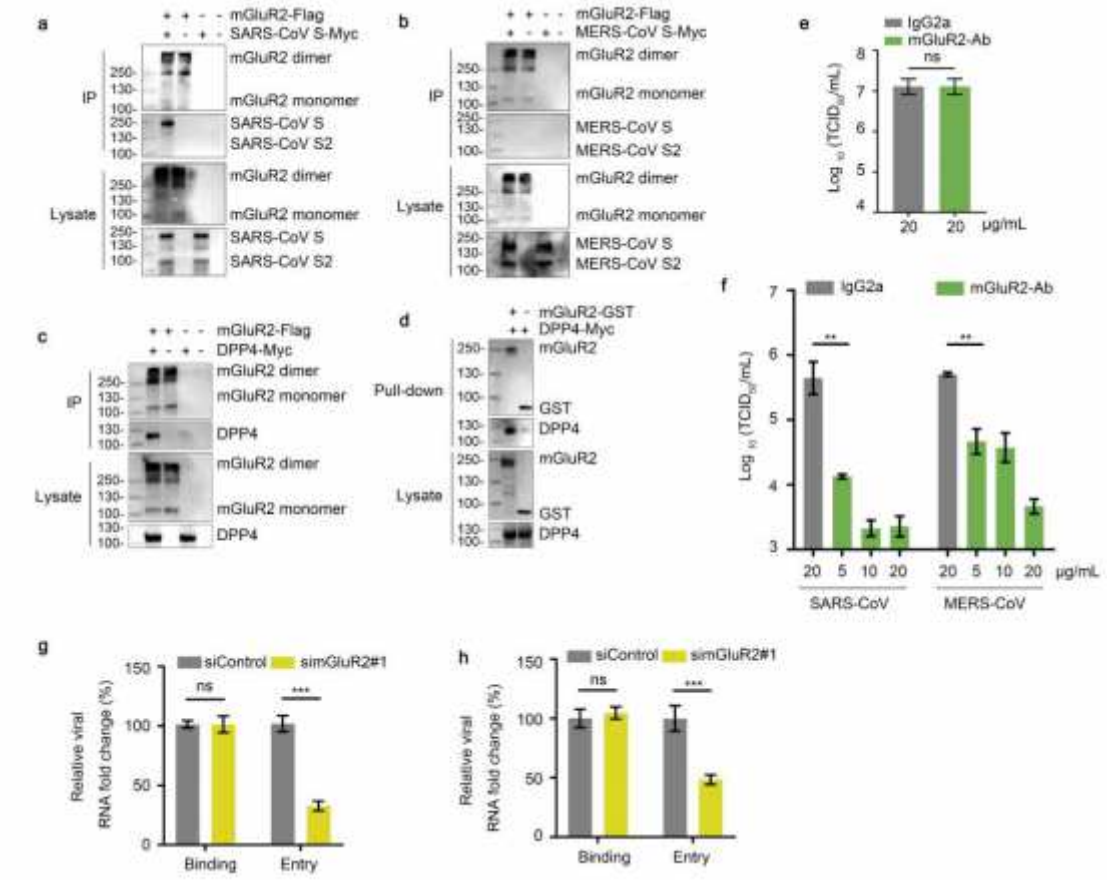

Figure 4

mGluR2 is important for both SARS-CoV S- and MERS-CoV-2 S-mediated endocytosis.